

# Surface Ligands Management for Efficient CsPbBr<sub>2</sub> Perovskite Nanocrystal Solar Cells

Chongming Liu, Qingsen Zeng, Yue Zhao, Yue Yu, Mingxi Yang, Hang Gao, Haotong Wei, and Bai Yang\*

CsPbX<sub>3</sub> (X = Cl, Br, I) inorganic perovskite nanocrystals (PNCs) not only maintain the excellent optical and electronic properties of bulk material but also possess the features of nano-materials, such as tunable bandgap and easily processable colloidal ink, and enable them to be suitable for incorporation into various electronic devices and compatible with printing techniques. In contrast to the traditional II–VI and III–V semiconductor nanocrystals, the unique defect-tolerance effect makes the CsPbX<sub>3</sub> PNCs promising materials for optoelectronic applications. The ligands around the PNCs play a critical role in the optoelectronic devices performance. Herein, through a facile hexane/ethyl acetate (MeOAc) solvent treatment method to control the ligand amount around CsPbBr<sub>2</sub> PNCs, the impact of ligand amount on the performance of solar cell is systematically demonstrated and the ligand amount is quantified precisely via the nuclear magnetic resonance internal standard method. Through controlling the ligand amount, the film quality, charge transfer, and transport properties are largely improved. In addition, a simple annealing process is applied to improve the interface properties by partial crystal fusion. As a consequence, the photovoltaic power conversion efficiency of 12.2% is achieved, which is the highest performance reported for mixed-halide CsPbX<sub>3</sub> PNCs solar cells.

The power conversion efficiency (PCE) of perovskite solar cells was improved quickly from less than 10% to over 25% in recent years<sup>[1]</sup> due to their excellent properties of direct bandgap,<sup>[2,3]</sup> high absorption coefficient,<sup>[4,5]</sup> narrower emission full width at half maximum,<sup>[6]</sup> low trap state density,<sup>[7–9]</sup> long diffusion length,<sup>[7,10]</sup> high carrier mobility, long carrier lifetimes,<sup>[11,12]</sup> etc. However, the stability of the organic part is still the major concern for its further commercialization, and the solubility of

pure inorganic perovskite is limited in solvents, which limits the corresponding device fabrication processes by solution processes.<sup>[13,14]</sup> Inorganic CsPbX<sub>3</sub> perovskite nanocrystals (PNCs), where X = Cl, Br, and I or mixed halide, were synthesized to improve the solubility by capping surface ligands on the nanoparticle, which provides a feasible and convenient way to fabricate inorganic perovskite device from solution processes.<sup>[15]</sup>


In contrast to the traditional II–VI and III–V semiconductor nanocrystals (NCs), PNCs show unique features: 1) They show the facile and low-cost synthesis method (inexpensive precursors, low temperature, and ambient conditions).<sup>[16,17]</sup> 2) Bandgap from ultraviolet (UV) to near infrared can be also tuned by halide composition management in addition to the quantum-size effect.<sup>[18]</sup> 3) Their peculiar electronic structure and dynamic lattice effects make the structure defects benign and their optical/electronic property is tolerant to the defects, as so-called defect-tolerance

effect.<sup>[19]</sup> Based on all these advantages, the PNCs have a promising prospect in optoelectronic applications including photodetectors,<sup>[20,21]</sup> light-emitting diodes,<sup>[22]</sup> lasers,<sup>[23]</sup> and solar cell (SC).<sup>[24–26]</sup> In 2016, the Luther group first reported the CsPbI<sub>3</sub> PNC SC fabricated through the layer-by-layer deposition method with a PCE of 10.77%,<sup>[24]</sup> approaching state-of-the-art PbS NCs SCs that have been developed for many years.<sup>[27]</sup> The high crystallinity of PNCs allows for the separation of crystallization and film-forming processes to ensure excellent film quality with good reproducibility.<sup>[28–30]</sup> Thus, the PNCs show a huge developing potential and prospect in practical photovoltaic device applications, especially for the printable devices, but the PNC device performance lags far away from the inorganic solar cell fabricated by the conventional one-step spin coating.<sup>[31,32]</sup> The major drawback is the poor electrical coupling that resulted from the interfaces between the NCs, which hinders the charge transport and thus collection in the PNC SC.<sup>[30]</sup> Therefore, to further improve the device performance, the surface chemical manipulation is critical.

To maintain the solubility and the stability of the NCs, non-conductive organic long-chain ligand oleic acid (OA) and oleylamine (OLA) remain in the interfaces, which increase the interparticle spacing and can be regarded as a fatal baffle for carrier.<sup>[30,33]</sup> A ligand exchange method during film deposition

C. Liu, Dr. Q. Zeng, Y. Zhao, Y. Yu, M. Yang, H. Gao, Prof. H. Wei, Prof. B. Yang  
State Key Laboratory of Supramolecular Structure and Materials  
College of Chemistry  
Jilin University  
Changchun 130012, P. R. China  
E-mail: byangchem@jlu.edu.cn

Prof. B. Yang  
State Key Laboratory of Applied Optics  
Changchun Institute of Optics Fine, Mechanics and Physics  
Chinese Academy of Sciences  
Changchun 130033, P. R. China

 The ORCID identification number(s) for the author(s) of this article can be found under <https://doi.org/10.1002/solr.202000102>.

DOI: 10.1002/solr.202000102

is promising, as the PCE increased to 13.4% from 8.5%, as reported by Luther.<sup>[30,34]</sup> A Cs salts post-treatment can also improve the electron coupling, as reported by Ma et al. As the carrier lifetime, diffusion length, and mobility of the treated CsPbI<sub>3</sub> NCs film were all improved, a 14.10% PCE was demonstrated, which is the highest in CsPbX<sub>3</sub> PNCs SCs.<sup>[28]</sup> To reduce the interfaces between the NCs, our group promoted the grain growth by post annealing the CsPbBrI<sub>2</sub> NCs film. Thus, a highest PCE 12.02% and a highest open-circuit voltage ( $V_{oc}$ ) 1.32 V were achieved.<sup>[35]</sup>

Here, in contrast to the ligand exchange or post-treatment, we report a more convenient and effective hexane/ethyl acetate (MeOAc) solvent treatment method to control the amount of the ligands around the initial CsPbBrI<sub>2</sub> NCs in the film. The corresponding device performance was improved with good reproducibility. We focus on the influence of ligand amount on the device performance, which has not been studied, and quantify the amount of ligands around NCs during the treatments by the nuclear magnetic resonance (NMR) internal standard method. Through controlling the ligand amount around the initial NCs, we realized a high-quality film with good charge transportation. Moreover, the trap state density decreased about fourfolds and the carrier mobility increased nearly 15-folds. Finally, the corresponding device performance increased from 5.9 to 12.2% after simple solvent treatment, which is one of the highest value in solar cells fabricated through inorganic PNCs. This work demonstrated that ligands around the PNCs play a critical role in further improving the PNCs' technique device performance.

The ligands binding to the NC surface is highly dynamic; thus, it is convenient to control the amount of ligands or oleyl species around the NCs by the repeated hexane/ethyl acetate (MeOAc) solvent treatment.<sup>[36]</sup> **Figure 1** shows the photos of CsPbBrI<sub>2</sub> NCs dissolved in hexane with (left) and without (right) UV excitation. When the purification was conducted more than three times, the NCs precipitate obviously due to low solubility caused by the serious ligand loss and NCs aggregation, which is unsuitable for device fabrication. Thus, we mainly focus on the device performance of the 1–3 times-treated NCs.

The ligand amount after solvent treatment was studied by NMR in deuterated chloroform. **Figure 2a** shows the full <sup>1</sup>H NMR spectrum and **Figure 2b** is the amplified <sup>1</sup>H NMR spectrum at

the chemical shift 4.8–6.0. The origin of the resonance peak is shown in **Figure 2c**, referring to previous work.<sup>[37]</sup> One-time treatment is obviously insufficient. The clear resonance 1 indicates the existence of the oleyl species (octadecylene [ODE], OA, and OLA), and the reaction solvent of ODE still remains, as the characteristic resonance 3 of ODE shows. After the two-time treatment was conducted, oleyl species was removed effectively and only a weak resonance peak signal of the solvent ODE was detected. When the treatment was repeated three times, most of the oleyl species was removed and the characteristic resonances 6 and 7 of OA almost disappear. At the same time, the treated NCs still maintain good solubility, as shown in **Figure 1**. To further determine the amount of oleyl species around the NCs, we used benzene as the standard substance to conduct the internal standard method, because benzene only shows a single resonance peak at 7.36 ppm in deuterated chloroform without resonances coinciding with the oleyl species. (Five parallel experiments were conducted to ensure the accuracy, detailed information is shown in Table S1, Supporting Information) We calculated the ligand amount based on Equation (1)<sup>[38,39]</sup>

$$N_l = N_s \times \frac{A_l}{A_s} \times \frac{P_s}{P_l} \quad (1)$$

where  $N$ ,  $A$ , and  $P$  are molar number, integral area of the quantitative chemical shift peak, and the corresponding proton number of the integrated peak, respectively. The subscripts  $l$  and  $s$  are abbreviations of ligand and standard substance benzene, respectively. The quantitative chemical shift peak of ligands is resonance peak 5. The calculated ligand amount of one, two, and three times-treated NCs are 2.35, 1.87, and 1.01 wt%, respectively, which means the hexane/MeOAc-mixed solvent treatment can effectively remove the ligands around NCs. To discuss clearly in the following paragraphs, we use the ligand amount as the subscript to present the NCs. Thus, NC<sub>2.35</sub>, NC<sub>1.87</sub>, and NC<sub>1.01</sub> represent the NCs treated for one, two, and three times, respectively.

**Figure 3a,b** shows the UV–visible (UV–vis) optical absorbance spectra and photoluminescence (PL) spectra of NC<sub>2.35</sub>, NC<sub>1.87</sub>, and NC<sub>1.01</sub>, respectively. Both the absorption peak and the PL peak redshift obviously as the ligand amount is reduced. We ascribe the redshift to the growth of NCs after treatments. Without the protection of sufficient ligands, the soft ionic crystal

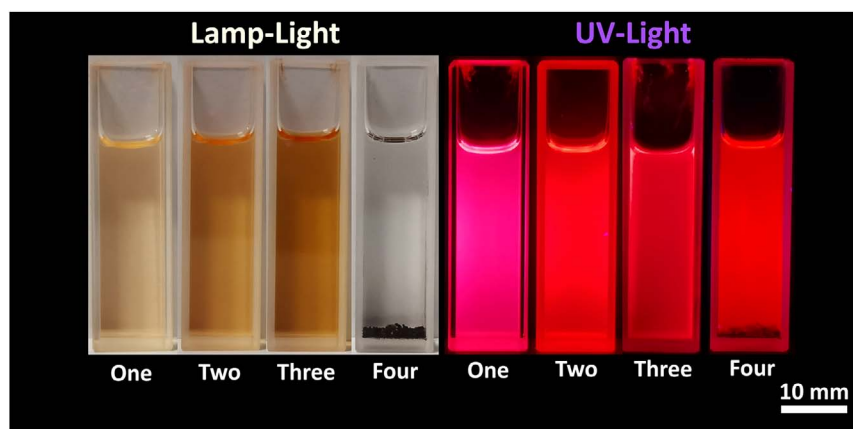


**Figure 1.** Photographs of CsPbBrI<sub>2</sub> NCs in hexane without (left) and with (right) UV light excitation after 1–4 times' treatments.

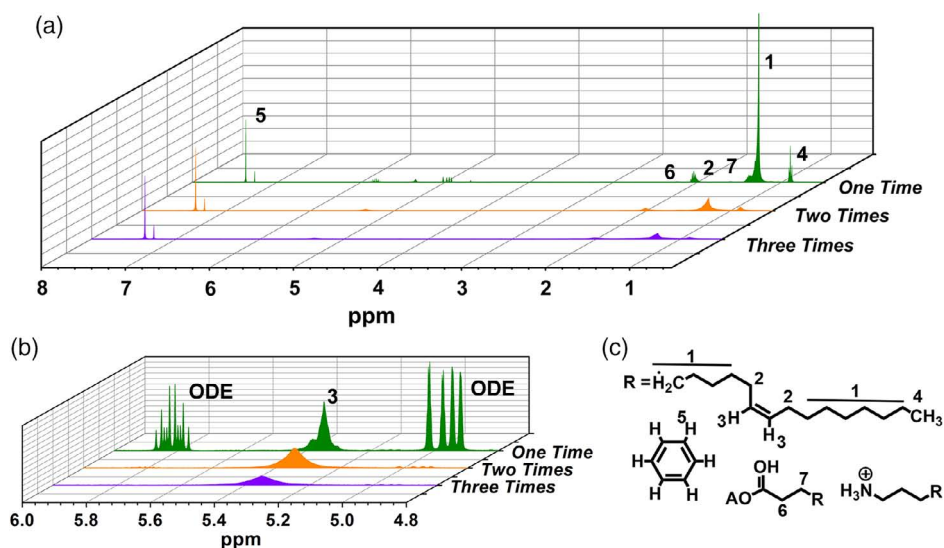


**Figure 2.** a) Full  $^1\text{H}$  NMR spectrum and b) enlarged spectrum of the 1–3 times' treatments of  $\text{CsPbBr}_2$  NCs in deuterated chloroform. c) The molecular structure of the corresponding resonance peak, as the number marked in (a). Note that the resonance peak intensity is normalized according to the intensity of standard substance benzene characteristic resonance peak at 7.36 ppm.

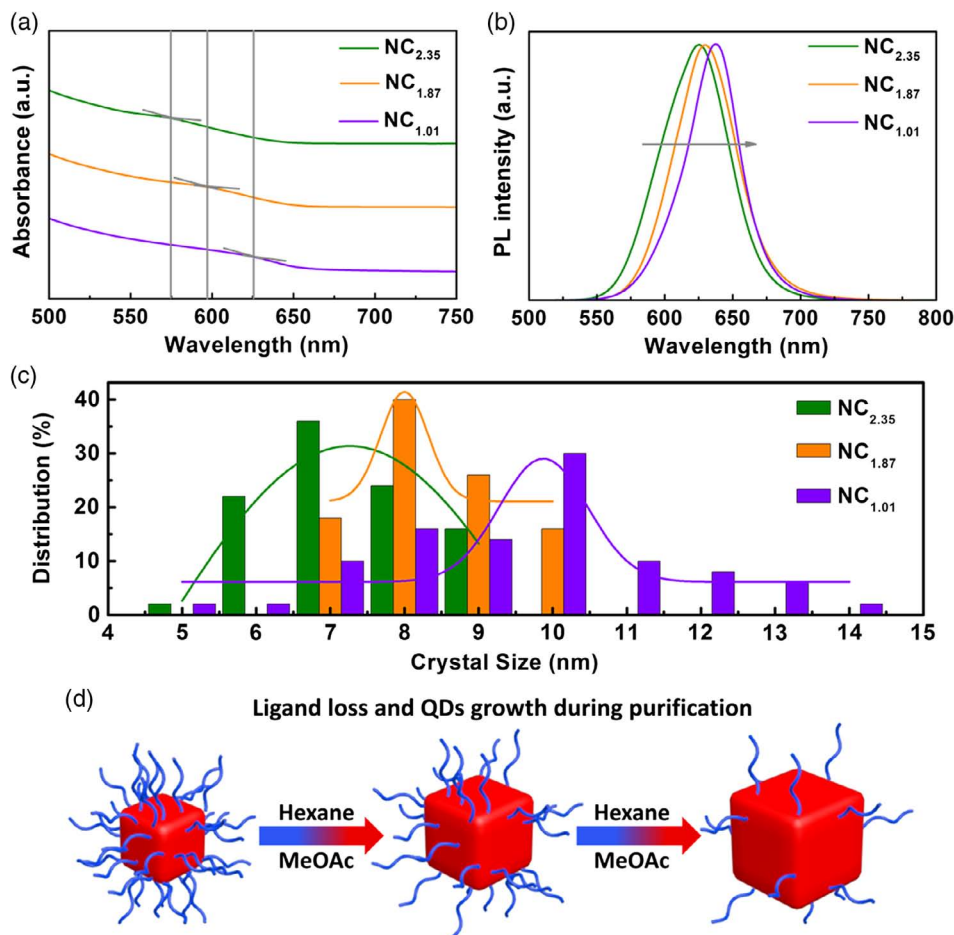


**Figure 3.** a) The steady-state PL spectra and b) UV-vis absorption spectra of  $\text{NC}_{2.35}$ ,  $\text{NC}_{1.87}$ , and  $\text{NC}_{1.01}$ . c) The crystal size distribution of  $\text{NC}_{2.35}$ ,  $\text{NC}_{1.87}$ , and  $\text{NC}_{1.01}$ . d) The schematic illustration of NCs changes during treatments.

structure makes the crystal easily grow. The average crystal size increases from 7.8 to 10.1 nm (Figure 3c). When the treatment time increases to three, the crystal size of NC<sub>1.01</sub> distributes widely due to the extremely weak ligand protection. The transmission electron microscopy (TEM) images of the 1–4-times treated NCs are shown in Figure S1, Supporting Information. Four times-treated NCs exhibit serious aggregation. The NCs fusion process is shown in Figure 3d. The size of NCs gradually enlarges due to the loss of surface ligands.

We fabricated the corresponding device of solvent-treated NCs via the layer-by-layer method. In brief, after spin coating the NCs as a film, the film was dipped into a Pb(OAc)<sub>2</sub>-saturated isopropanol solution and simply rinsed by anhydrous MeOAc to partially remove the insulating ligands. The process was repeated four times to obtain the film with desired thickness. Figure 4a shows the reverse-scan density–voltage (*J*–*V*) curves of NC devices and the device structure Glass/ITO/TiO<sub>2</sub>/Perovskite/P3HT/Au. The corresponding external quantum efficiency and integrated current density curves are shown in Figure S2, Supporting Information. The PCEs of NC<sub>2.35</sub>, NC<sub>1.87</sub>, and NC<sub>1.01</sub> are 5.9%, 8.9%, and 12.2%, respectively. The corresponding detailed device performance is shown in Table 1. The NC<sub>1.01</sub> device exhibits the best performance, which is one of the highest solar cell via PNCs' device techniques (Figure 4b and Table S2, Supporting Information). The champion device forward-scan PCE is 8.5% (Figure S2, Supporting Information), with a stabilized power output 10.2%. The large hysteresis may come from the ionic

**Table 1.** Champion device performance parameters of NCs with different ligand amounts.

NC <sub>ligand amount</sub>	<i>J</i> <sub>sc</sub> [mA cm <sup>−2</sup> ]	<i>V</i> <sub>oc</sub> [V]	FF [%]	PCE [%]
NC <sub>2.35</sub>	7.86	1.14	65.4	5.9
NC <sub>1.87</sub>	11.86	1.19	63.2	8.9
NC <sub>1.01</sub>	14.22	1.20	71.3	12.2

accumulation at the charge extraction interfaces due to external bias.<sup>[40,41]</sup> In contrast to the NC<sub>2.35</sub> devices, the NC<sub>1.87</sub> or NC<sub>1.01</sub> devices show a higher open-circuit voltage (*V*<sub>oc</sub>). The same trend can be further demonstrated in the statistical distribution of photovoltaic parameters (Figure S3, Supporting Information). Moreover, the short-circuit current density (*J*<sub>sc</sub>) and fill factor (FF) also gradually increase.

The improvement of device performance mainly results from an enhanced *J*<sub>sc</sub>. We first compare the UV–vis absorption spectra of the three fabricated films (Figure 4d). The promoted light absorption intensity with the decreased ligand amount coincides with the enhanced *J*<sub>sc</sub>. A sample dipping and rinsing process can only partially remove the native ligands. But when the ligands distribute around NCs densely, the protection for NCs is strong and the solubility of the NCs will remain in good status after film deposition.<sup>[30]</sup> During the following film deposition, the NCs on the previous deposited film will be redispersed in the

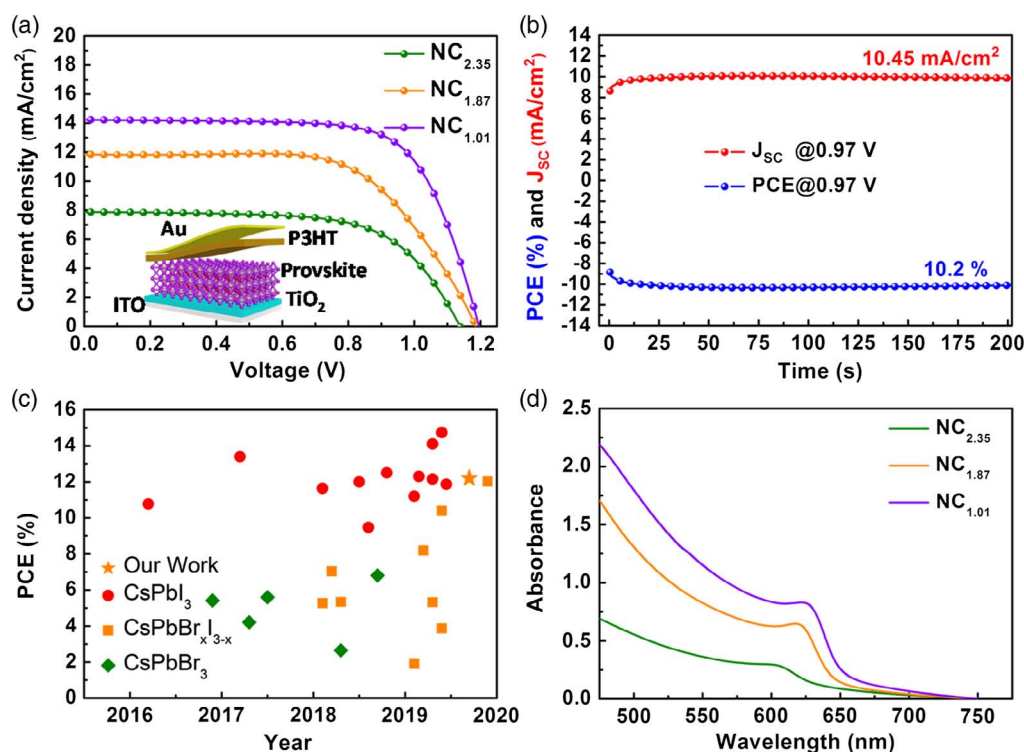


**Figure 4.** a) The reverse-scan current density–voltage (*J*–*V*) curves of the champion device fabricated by NC<sub>2.35</sub>, NC<sub>1.87</sub>, and NC<sub>1.01</sub>. The inset presents the device architecture structure. The PCE was measured at 100 mW cm<sup>−2</sup> AM 1.5G illumination, which was corrected by a calibrated Si solar cell. b) The champion solar cell stabilized the power output measurement held at a constant voltage of 0.97 V (PCE in blue; current density in red). c) PCE distributions of different solar cells fabricated by PNCs based on this and previous work. d) UV–vis absorption spectra of the annealed CsPbBr<sub>2</sub> NCs films.



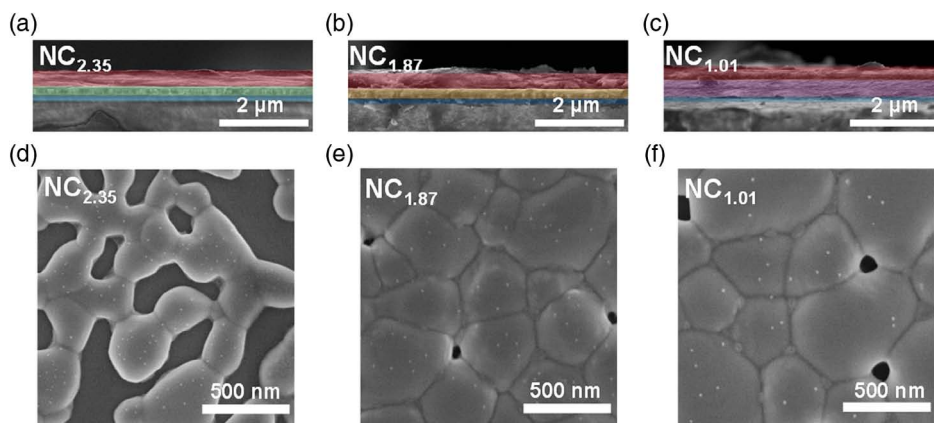


**Figure 5.** Device structure (bottom to top: TiO<sub>2</sub>/CsPbBr<sub>2</sub>/P3HT) cross-sectional SEM images of a) NC<sub>2.35</sub>, b) NC<sub>1.87</sub>, and c) NC<sub>1.01</sub>. SEM images of the annealed CsPbBr<sub>2</sub> film fabricated by d) NC<sub>2.35</sub>, e) NC<sub>1.87</sub>, and f) NC<sub>1.01</sub>.

spin-coating solvent, resulting in an unsatisfactory film thickness and even the film morphology. We show the scanning electron microscope (SEM) and cross-sectional SEM images in **Figure 5**. From **Figure 5a,b**, it is obvious that the film of NC<sub>1.01</sub> (343 nm) is thicker than that of NC<sub>2.35</sub> (210 nm) and NC<sub>1.87</sub> (220 nm), which ensures the sufficient absorption of the light. Though the film thickness of NC<sub>2.35</sub> and NC<sub>1.87</sub> is almost the same, the terrible morphology on the substrate of NC<sub>2.35</sub> will also reduce light absorption (**Figure 5c**), resulting in the lower  $J_{sc}$  than the NC<sub>1.87</sub> device. Thus the ligand amount plays an important role in the final film quality, which will be discussed in detail later.

A facile 330 °C annealing process of 2 min is applied to the spin-coated film to promote the crystal fusion and growth, known as Ostwald ripening.<sup>[42]</sup> Post-growth will reduce the interparticle spacing between the crystals and remove the grain boundaries. As the ligand amount around NCs was reduced, the final grain size after annealing becomes large (**Figure 5d–f**). It has been demonstrated that the large grain size is beneficial for device performance<sup>[43–45]</sup> and grain boundaries are detrimental to the photovoltaic properties of perovskites.<sup>[46]</sup> Though the pinholes on the film may affect the device performance by leakage current, a poly(3-hexylthiophene-2,5-diyl) (P3HT) spin coated on top can fill up them, showing a smooth morphology (**Figure S4**, Supporting Information). Energy-dispersive spectroscopy (EDS) confirms the Cs:Pb:Br:I elemental ratios of the annealed film to be 1:1.14:1.25:1.96 and the elements distribute uniformly throughout the film without phase separation, suggesting that the final film can be recognized as CsPbBrI<sub>2</sub> (**Figure S5**, Supporting Information). The white spots on the grains, which are too small to detect the exact composition, are probably CsBr, according to the previous work,<sup>[47,48]</sup> and it may play a positive role in the device performance, as recently reported by Qu and coworkers.<sup>[48]</sup> The X-ray diffraction (XRD) spectra feature the crystal structures of the three perovskite films, which indicate that all the samples are in the cubic perovskite phase (**Figure 6a**). The strong intensities of peaks at 14.6° and 29.5° are assigned to the [100] and [200] planes of CsPbBrI<sub>2</sub>, indicating the high-orientation crystallographic direction.<sup>[49]</sup> The ligand amount has no influence on the crystal growth direction. In terms of the

significantly stronger XRD intensity, this is in good agreement with larger grain size and thicker film,<sup>[43]</sup> exhibited in SEM images. We ascribe the enlarged grain size to the decreased ligand amount, reducing the hindrance of crystal growth.

To further investigate performance improvement, it is necessary to study the charge dynamics in devices with different ligand amounts. **Figure 6b** shows the Tauc plot of  $(Ah\nu)^{1/2}$  versus photon energy ( $h\nu$ ), converted from the UV–vis absorption in **Figure 4d**. The bandgaps ( $E_g$ ) of the three samples is approximately 1.92 eV. Combined with the valence band values of the three samples, calculated from the UV photoelectron spectroscopy (UPS) spectra (**Figure S6**, Supporting Information), the band alignment of the three devices is determined, as shown in **Figure 6c**. The energy levels of TiO<sub>2</sub> and P3HT are obtained from the previous work.<sup>[35,50]</sup> The evidently mismatched energy level of the NC<sub>2.35</sub> device will induce charge accumulation at the interface, resulting in the low charge extraction efficiency and charge recombination. Even worse, the difference of the electron quasi-Fermi level ( $E_{Fn}$ ) and the hole quasi-Fermi level ( $E_{Fp}$ ) will be smaller. This will cause a large energy loss, thus a low  $V_{oc}$ ,<sup>[51]</sup> which is in coincidence with the low  $V_{oc}$  of the NC<sub>2.35</sub> device.

We investigated the dark current density–voltage characteristics based on the electron-only devices (ITO/TiO<sub>2</sub>/Perovskite/PCBM/Au) in the dark. As shown in **Figure 7a–c**, the current density increases slowly with the voltage before the kink point, demonstrating an Ohmic response. In the next linear stage, the current density increases sharply, corresponding to a trap-filling response, which means the trap states are filled up with the injected charges, and the applied voltage at the kink point can be regarded as the trap-filled-limit voltage ( $V_{TFL}$ ).<sup>[52]</sup> The trap state density ( $N_t$ ) is calculated through Equation (2).

$$N_t = \frac{2\epsilon_0\epsilon_r V_{TFL}}{qL^2} \quad (2)$$

where  $\epsilon_0$  is the vacuum permittivity,  $\epsilon_r$  is the relative dielectric constant of CsPbBrI<sub>2</sub> ( $\epsilon_r = 8.5$ ),<sup>[53]</sup>  $q$  is the elemental charge, and  $L$  is the thickness of the film. The charge mobility ( $\mu$ ) can be estimated by the Mott–Gurney equation, as shown in Equation (3)<sup>[54]</sup>

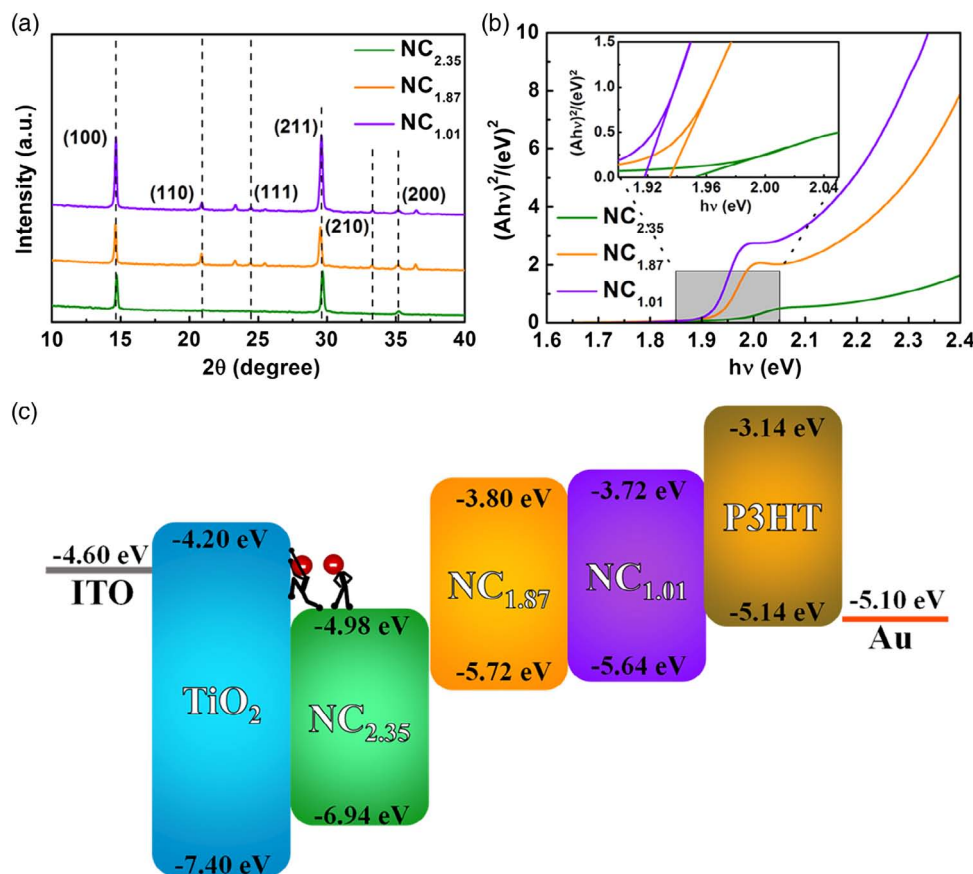


**Figure 6.** a) XRD patterns of the annealed CsPbBr<sub>2</sub> films prepared by NCs with different ligand amounts. b) Tauc plots of CsPbBr<sub>2</sub> layer deposited by NCs with different ligand amounts. c) Schematic energy-level diagram.

$$J = \frac{9\mu\epsilon_0\epsilon_r V_{\text{TFL}}^2}{8d^3} \quad (3)$$

where  $J$  is the current density. As the ligand amount decreases, the trap states decrease from  $4.48 \times 10^{16}$  to  $1.10 \times 10^{16} \text{ cm}^{-3}$  and the charge mobility increases from  $1.76 \times 10$  to  $2.59 \times 10^{-6} \text{ cm}^2 \text{ V}^{-1} \text{ S}^{-1}$ . The reduced trap density is attributed to the gradually increased FF.<sup>[55]</sup> We ascribe the reduced trap states and improved charge mobility to the fewer grain boundaries<sup>[51,56]</sup> as the defects at grain boundaries are critical to device performance.<sup>[46]</sup> The increased grain size also contributes to the improved charge mobility as the hopping numbers for the transport between the grains decrease.<sup>[57]</sup> The time-resolved PL (TRPL) measurements are carried out to determine the PL decay lifetimes. The results of TRPL are shown in Figure 7d and the detailed exponential fitting parameters are shown in Table S3, Supporting Information. The average lifetimes ( $\tau_{\text{ave}}$ ) of NC<sub>2.35</sub>, NC<sub>1.87</sub>, and NC<sub>1.01</sub> are 175, 451, and 795 ns, respectively.  $\tau_{\text{ave}}$  delays longer, suggesting the suppressed nonradiative recombination in the film.<sup>[49]</sup> It is also a strong evidence for the defect reduction.

Electrochemical impedance spectra (EIS) measurements are carried out in the dark at the bias of 0 V with a frequency ranging from 1 mHz to 200 kHz. Figure 7e shows the Nyquist plot with mainly one semicircle. The inset is the equivalent circuit and can be described as Equation (4).<sup>[58]</sup>

$$\left[ Z' - \left( R_s + \frac{R_{\text{sh}}}{2} \right)^2 \right] + (Z'')^2 = \left( \frac{R_{\text{sh}}}{2} \right)^2 \quad (4)$$

where  $Z'$  and  $Z''$  are the impedance real and imaginary part. In this model, the series resistance ( $R_s$ ) is donated as the resistance of wire contacts and materials. The shunt resistance ( $R_{\text{sh}}$ ) is related to the loss of carriers.<sup>[59,60]</sup> Take the device operation mechanism into account, after charge generation, charges transfer between grains and are transported to the collection layers, which means that each semicircle presents two process charge transfers and transportation. Thus,  $R_{\text{sh}}$  can be regarded as a charge recombination resistance at the grain/grain and perovskite/collection layers interfaces.<sup>[57,61]</sup> The enlarged  $R_{\text{sh}}$  value indicates the suppressed recombination process, which can be attributed to the better charge transfer and more efficient charge extraction.

In conclusion, we systematically study the ligand amount around the initial NCs and its influence on the device performance. Proper ligand amount is necessary for the excellent device performance. An extremely low ligand amount will destroy the solubility of the NCs, inducing serious trouble in film formation. A high ligand amount will lead to an unsatisfactory morphology and further restrict the NC growth during the post-annealing process. This will result not only in low light absorption but also bad charge dynamic behavior. Through

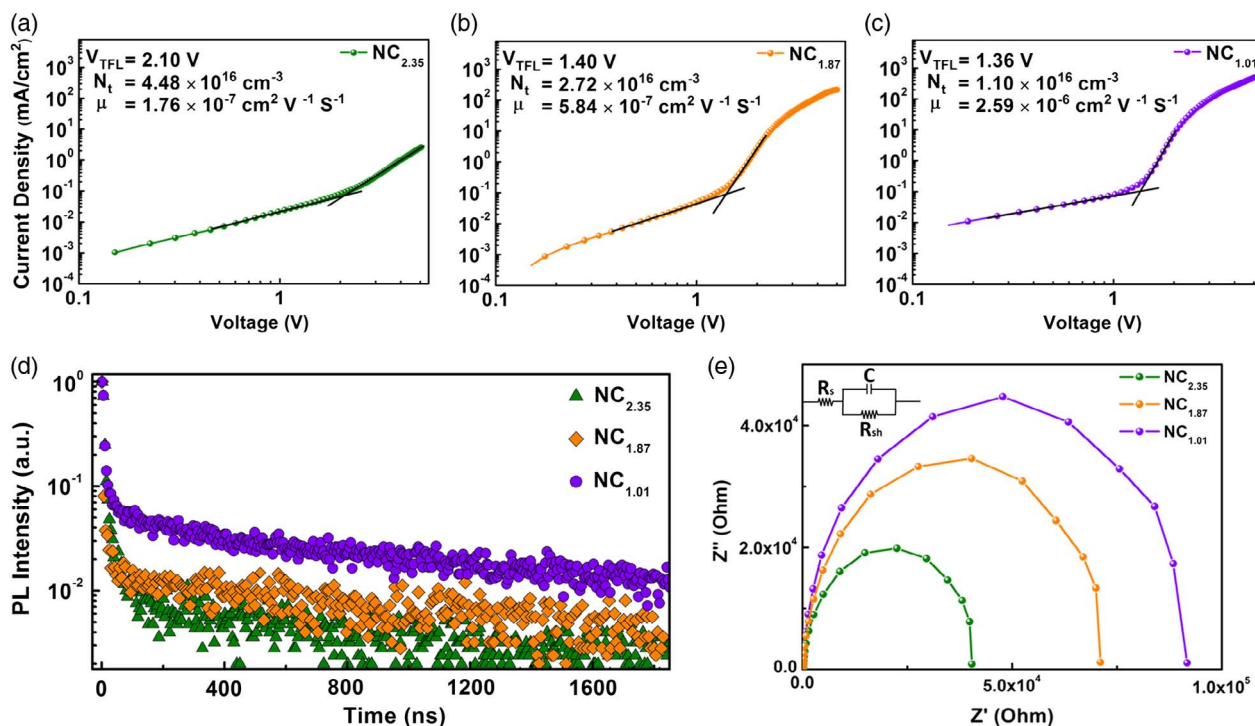


**Figure 7.** a) Dark  $J$ - $V$  measurements of the electron-only devices displaying  $V_{\text{TFL}}$  kink point behavior for NC<sub>2.35</sub>, b) NC<sub>1.87</sub>, and c) NC<sub>1.01</sub> device. d) PL decay curves of films fabricated by NCs with different ligand amounts. e) Nyquist plots for devices with an applied bias of 0 V in the dark condition for NCs with different ligand amounts. The inset is the equivalent electrical circuit diagram for the analysis of charge dynamics.

precisely controlling the ligand amount around the NCs at 1.01 wt%, the corresponding solar cell exhibits a PCE as high as 12.2%, which is one of the highest device performances fabricated by CsPbX<sub>3</sub> PNC techniques. This work highlights the importance of controlling the ligand amount around PNCs in the PNCs-based device performance.

## Experimental Section

**Synthesis of Cs Oleate Precursor:** About 0.75 g of Cs<sub>2</sub>CO<sub>3</sub>, 3 mL of OA, and 75 mL of 1-octadecene (ODE) were added to a 250 mL three-necked round bottom flask. The reaction mixture was stirred in vacuum for about 2 h at 120 °C. The reaction was completed when the solution was clear, indicating that Cs<sub>2</sub>CO<sub>3</sub> reacted with the OA. The Cs oleate solution in ODE was stored in N<sub>2</sub> until it was needed for NCs synthesis.

**Synthesis of CsPbBr<sub>2</sub> NCs:** About 50 mL of ODE, 0.700 g of PbI<sub>2</sub>, and 0.239 g of PbBr<sub>2</sub> were added into a 250 mL three-necked flask; then, it was stirred in vacuum for about 1 h at 120 °C. About 5 mL of dried OA and 5 mL of dried OLA (5 mL) were injected to the flask at 120 °C. When the solution became clear, the temperature was increased to 180 °C and 8 mL of Cs oleate (preheated to about 70 °C) precursor was quickly injected. After 5–10 s, the reaction mixture was cooled down to room temperature by an ice–water bath. For first-time purification, the synthesized CsPbBr<sub>2</sub> NCs were precipitated by adding methyl acetate (MeOAc) at the volume ratio of NCs reaction solution: MeOAc was 1:1.86 and then centrifuged at 8500 rpm for 5 min. For two-times purification, the precipitate of first-time purification was redispersed in 12 mL of hexane and precipitated by adding 30 mL of MeOAc (volume ratio of NC solution: MeOAc = 1:2.5); it was centrifuged again for 5 min at 8500 rpm. As for the three or more times of purification, the precipitated NCs were redispersed in 4 mL of hexane and then precipitated by adding 10 mL MeOAc at the volume ratio

1:2.5. Finally, the one/two/three times-purified CsPbBr<sub>2</sub> NCs were redispersed in toluene at a concentration of 80 mg mL<sup>-1</sup> and stored in a freezer at 4 °C for device fabrication.

**Device Fabrication:** The prepatterned ITO was cleaned using chloroform, acetone, isopropanol, and ethanol step by step before drying in N<sub>2</sub> flow. Next, the ITO substrate was coated with the TiO<sub>2</sub> precursor at a speed of 2000 rpm. The TiO<sub>2</sub> precursors were prepared, according to a previous work.<sup>[57]</sup> The TiO<sub>2</sub>-coated ITO substrate was annealed at 455 °C for 20 min. The CsPbI<sub>2</sub>Br photoactive layer was deposited using the procedure described later, resulting in a total thickness of 200–350 nm. The samples were put onto a hotplate at 330 °C for 2 min in a glove box. After cooling down to room temperature, the P3HT hole-transporting material (15 mg P3HT in 1 mL chlorobenzene) was spin cast at 2000 rpm for 30 s, following 5 min annealing at 200 °C. Finally, a 25 nm gold electrode was evaporated through a mask at a pressure below 10<sup>-5</sup> Torr.

**CsPbI<sub>2</sub>Br NCs Film Deposition:** The processes were conducted in air ambient at a relative humidity <15%. The film was deposited similar to a previous work with some improvement.<sup>[24]</sup> Ligand solutions were made by sonicating 30 mg of Pb(OAc)<sub>2</sub> in 30 mL of anhydrous IPA for 5 min. The solution was stored for 2 days to precipitate the excess salt. The CsPbI<sub>2</sub>Br NCs were spin cast on the substrate at 850–1000 rpm for 20 s followed by 2000 rpm for 10 s and then soaked in the ligand solution for 10 s to remove long-chain ligands. The film was rinsed using neat, anhydrous MeOAc for 5 s and then dried with a stream of air. This procedure was repeated multiple four times to build up 100–300 nm-thick films.

## Supporting Information

Supporting Information is available from the Wiley Online Library or from the author.

## Acknowledgements

This work was financially supported by the National Science Foundation of China (NSFC) under grant no. 51433003, the National Key Research and Development Program of China (2016YFB0401701), the Fundamental Research Funds for the Central Universities, JLU and JLUSTRIT (2017TD-06), the Opening Funds of State Key Laboratory of Applied Optics, Changchun Institute of Optics, Fine Me-chanics and Physics, Chinese Academy of Science, and the China Postdoctoral Science Foundation under grant no. 2019M661202.

## Conflict of Interest

The authors declare no conflict of interest.

## Keywords

CsPbBr<sub>2</sub>, inorganic perovskites, ligand amount control, nanocrystals, solar cells

Received: February 24, 2020

Revised: March 9, 2020

Published online: March 25, 2020

- [1] National Renewable Energy Laboratory, Best Research-Cell Efficiency Chart, <https://www.nrel.gov/pv/device-performance.html> (accessed: February 2020).
- [2] C. Li, H. Wang, F. Wang, T. Li, M. Xu, H. Wang, Z. Wang, X. Zhan, W. Hu, L. Shen, *Light Sci. Appl.* **2020**, 9, 31.
- [3] W. Hu, H. Cong, W. Huang, Y. Huang, L. Chen, A. Pan, C. Xue, *Light Sci. Appl.* **2019**, 8, 106.
- [4] L. Gu, Z. Fan, *Light Sci. Appl.* **2017**, 6, e17090.
- [5] S. B. Kang, J.-H. Kim, M. H. Jeong, A. Sanger, C. U. Kim, C.-M. Kim, K. J. Choi, *Light Sci. Appl.* **2019**, 8, 121.
- [6] H.-W. Chen, R.-D. Zhu, J. He, W. Duan, W. Hu, Y.-Q. Lu, M.-C. Li, S.-L. Lee, Y.-J. Dong, S.-T. Wu, *Light Sci. Appl.* **2017**, 6, e17043.
- [7] Q. Dong, Y. Fang, Y. Shao, P. Mulligan, J. Qiu, L. Cao, J. Huang, *Science* **2015**, 347, 967.
- [8] D. Yang, X. Li, W. Zhou, S. Zhang, C. Meng, Y. Wu, Y. Wang, H. Zeng, *Adv. Mater.* **2019**, 31, e1900767.
- [9] H. Sun, Z. Yang, M. Wei, W. Sun, X. Li, S. Ye, Y. Zhao, H. Tan, E. L. Kynaston, T. B. Schon, H. Yan, Z. H. Lu, G. A. Ozin, E. H. Sargent, D. S. Seferos, *Adv. Mater.* **2017**, 29, 1701153.
- [10] S. Zhang, W. Chen, S. Wu, R. Chen, Y. Huang, Z. Yang, J. Li, L. Han, W. Chen, *J. Mater. Chem. A* **2019**, 7, 18603.
- [11] H. H. Fang, F. Wang, S. Adjokatse, N. Zhao, J. Even, M. Antonietta Loi, *Light Sci. Appl.* **2016**, 5, e16056.
- [12] C. Xie, P. You, Z. Liu, L. Li, F. Yan, *Light Sci. Appl.* **2017**, 6, e17023.
- [13] Y. C. Zhao, W. K. Zhou, X. Zhou, K. H. Liu, D. P. Yu, Q. Zhao, *Light Sci. Appl.* **2017**, 6, e16243.
- [14] S. Zhang, S. Wu, W. Chen, H. Zhu, Z. Xiong, Z. Yang, C. Chen, R. Chen, L. Han, W. Chen, *Mater. Today Energy* **2018**, 8, 125.
- [15] L. Protesescu, S. Yakunin, M. I. Bodnarchuk, F. Krieg, R. Caputo, C. H. Hendon, R. X. Yang, A. Walsh, M. V. Kovalenko, *Nano Lett.* **2015**, 15, 3692.
- [16] Q. Zhang, Y. Yin, *ACS Cent. Sci.* **2018**, 4, 668.
- [17] M. V. Kovalenko, L. Protesescu, M. I. Bodnarchuk, *Science* **2017**, 358, 745.
- [18] C. de Weerd, T. Gregorkiewicz, L. Gomez, *Adv. Opt. Mater.* **2018**, 6, 1800289.
- [19] Q. A. Akkerman, G. Raino, M. V. Kovalenko, L. Manna, *Nat. Mater.* **2018**, 17, 394.
- [20] P. Ramasamy, D. H. Lim, B. Kim, S. H. Lee, M. S. Lee, J. S. Lee, *Chem. Commun.* **2016**, 52, 2067.
- [21] C. H. Kang, I. Dursun, G. Liu, L. Sinatra, X. Sun, M. Kong, J. Pan, P. Maity, E.-N. Ooi, T. K. Ng, O. F. Mohammed, O. M. Bakr, B. S. Ooi, *Light Sci. Appl.* **2019**, 8, 94.
- [22] J. Song, J. Li, X. Li, L. Xu, Y. Dong, H. Zeng, *Adv. Mater.* **2015**, 27, 7162.
- [23] Y. Wang, X. Li, J. Song, L. Xiao, H. Zeng, H. Sun, *Adv. Mater.* **2015**, 27, 7101.
- [24] A. Swarnkar, A. R. Marshall, E. M. Sanehira, B. D. Chernomordik, D. T. Moore, J. A. Christians, T. Chakrabarti, J. M. Luther, *Science* **2016**, 354, 92.
- [25] Q. Wang, Z. Jin, D. Chen, D. Bai, H. Bian, J. Sun, G. Zhu, G. Wang, S. F. Liu, *Adv. Energy Mater.* **2018**, 8, 1800007.
- [26] X. Zhang, Z. Jin, J. Zhang, D. Bai, H. Bian, K. Wang, J. Sun, Q. Wang, S. F. Liu, *ACS Appl. Mater. Interfaces* **2018**, 10, 7145.
- [27] S.-W. Baek, S. Jun, B. Kim, A. H. Proppe, O. Ouellette, O. Voznyy, C. Kim, J. Kim, G. Walters, J. H. Song, S. Jeong, H. R. Byun, M. S. Jeong, S. Hoogland, F. P. Garcia de Arquer, S. O. Kelley, J.-Y. Lee, E. H. Sargent, *Nat. Energy* **2019**, 4, 969.
- [28] X. Ling, S. Zhou, J. Yuan, J. Shi, Y. Qian, B. W. Larson, Q. Zhao, C. Qin, F. Li, G. Shi, C. Stewart, J. Hu, X. Zhang, J. M. Luther, S. Duhm, W. Ma, *Adv. Energy Mater.* **2019**, 9, 1900721.
- [29] J. Yuan, X. Ling, D. Yang, F. Li, S. Zhou, J. Shi, Y. Qian, J. Hu, Y. Sun, Y. Yang, X. Gao, S. Duhm, Q. Zhang, W. Ma, *Joule* **2018**, 2, 2450.
- [30] E. M. Sanehira, A. R. Marshall, J. A. Christians, S. P. Harvey, P. N. Ciesielski, L. M. Wheeler, P. Schulz, L. Y. Lin, M. C. Beard, J. M. Luther, *Sci. Adv.* **2017**, 3, eaao4204.
- [31] Y. Wang, X. Liu, T. Zhang, X. Wang, M. Kan, J. Shi, Y. Zhao, *Angew. Chem.* **2019**, 58, 16691.
- [32] Y. Wang, M. I. Dar, L. K. Ono, T. Zhang, M. Kan, Y. Li, L. Zhang, X. Wang, Y. Yang, X. Gao, Y. Qi, M. Gratzel, Y. Zhao, *Science* **2019**, 365, 591.
- [33] K. Chen, Q. Zhong, W. Chen, B. Sang, Y. Wang, T. Yang, Y. Liu, Y. Zhang, H. Zhang, *Adv. Funct. Mater.* **2019**, 29, 1900991.
- [34] L. M. Wheeler, E. M. Sanehira, A. R. Marshall, P. Schulz, M. Suri, N. C. Anderson, J. A. Christians, D. Nordlund, D. Sokaras, T. Kroll, S. P. Harvey, J. J. Berry, L. Y. Lin, J. M. Luther, *J. Am. Chem. Soc.* **2018**, 140, 10504.
- [35] Q. Zeng, X. Zhang, X. Feng, S. Lu, Z. Chen, X. Yong, S. A. T. Redfern, H. Wei, H. Wang, H. Shen, W. Zhang, W. Zheng, H. Zhang, J. S. Tse, B. Yang, *Adv. Mater.* **2018**, 30, 1705393.
- [36] J. De Roo, M. Ibanez, P. Geiregat, G. Nedelcu, W. Walravens, J. Maes, J. C. Martins, I. Van Driessche, M. V. Kovalenko, Z. Hens, *ACS Nano* **2016**, 10, 2071.
- [37] J. Li, L. Xu, T. Wang, J. Song, J. Chen, J. Xue, Y. Dong, B. Cai, Q. Shan, B. Han, H. Zeng, *Adv. Mater.* **2017**, 29, 201603885.
- [38] A. Wu, J. Yu, J. Zhuang, Q. Ning, *Chin. J. Anal. Chem.* **2006**, 34, 695.
- [39] X. Sun, L. Wu, *J. Appl. Polym. Sci.* **2011**, 121, 3246.
- [40] F. Wu, R. Pathak, K. Chen, G. Wang, B. Bahrami, W.-H. Zhang, Q. Qiao, *ACS Energy Lett.* **2018**, 3, 2457.
- [41] S. N. Habisreutinger, N. K. Noel, H. J. Snaith, *ACS Energy Lett.* **2018**, 3, 2472.
- [42] J. K. Nam, M. S. Jung, S. U. Chai, Y. J. Choi, D. Kim, J. H. Park, *J. Phys. Chem. Lett.* **2017**, 8, 2936.
- [43] D. Bai, H. Bian, Z. Jin, H. Wang, L. Meng, Q. Wang, S. Liu, *Nano Energy* **2018**, 52, 408.
- [44] W. Chen, H. Chen, G. Xu, R. Xue, S. Wang, Y. Li, Y. Li, *Joule* **2019**, 3, 191.



- [45] P. Wang, X. Zhang, Y. Zhou, Q. Jiang, Q. Ye, Z. Chu, X. Li, X. Yang, Z. Yin, J. You, *Nat. Commun.* **2018**, 9, 2225.
- [46] H. Uratani, K. Yamashita, *J. Phys. Chem. Lett.* **2017**, 8, 742.
- [47] Q. Ma, S. Huang, S. Chen, M. Zhang, C. F. J. Lau, M. N. Lockrey, H. K. Mulmudi, Y. Shan, J. Yao, J. Zheng, X. Deng, K. Catchpole, M. A. Green, A. W. Y. Ho-Baillie, *J. Phys. Chem. C* **2017**, 121, 19642.
- [48] Y. Zhang, C. Wu, D. Wang, Z. Zhang, X. Qi, N. Zhu, G. Liu, X. Li, H. Hu, Z. Chen, L. Xiao, B. Qu, *Sol. RRL* **2019**, 3, 1900254.
- [49] J. Yuan, L. Zhang, C. Bi, M. Wang, J. Tian, *Sol. RRL* **2018**, 2, 1800188.
- [50] E. H. Jung, N. J. Jeon, E. Y. Park, C. S. Moon, T. J. Shin, T. Y. Yang, J. H. Noh, J. Seo, *Nature* **2019**, 567, 511.
- [51] C. Liu, Q. Zeng, B. Yang, *Adv. Mater. Interfaces* **2019**, 6, 1901136.
- [52] K. Wang, Z. Jin, L. Liang, H. Bian, H. Wang, J. Feng, Q. Wang, S. Liu, *Nano Energy* **2019**, 58, 175.
- [53] H. Sun, J. Zhang, X. Gan, L. Yu, H. Yuan, M. Shang, C. Lu, D. Hou, Z. Hu, Y. Zhu, L. Han, *Adv. Energy Mater.* **2019**, 9, 1900896.
- [54] J. Han, X. Yin, Y. Zhou, H. Nan, Y. Gu, M. Tai, J. Li, H. Lin, *ACS Appl. Mater. Interfaces* **2018**, 10, 42328.
- [55] X. Meng, C. H. Y. Ho, S. Xiao, Y. Bai, T. Zhang, C. Hu, H. Lin, Y. Yang, S. K. So, S. Yang, *Nano Energy* **2018**, 52, 300.
- [56] D. Meggiolaro, S. G. Motti, E. Mosconi, A. J. Barker, J. Ball, C. Andrea Riccardo Perini, F. Deschler, A. Petrozza, F. De Angelis, *Energy Environ. Sci.* **2018**, 11, 702.
- [57] Q. Zeng, Z. Chen, F. Liu, G. Jin, X. Du, T. Ji, Y. Zhao, Y. Yue, H. Wang, D. Meng, T. Xie, H. Zhang, B. Yang, *Sol. RRL* **2017**, 1, 1600020.
- [58] B. Yu, H. Zhang, J. Wu, Y. Li, H. Li, Y. Li, J. Shi, H. Wu, D. Li, Y. Luo, Q. Meng, *J. Mater. Chem. A* **2018**, 6, 19810.
- [59] H. Li, J. Cao, Q. Zhou, L. Ding, J. Wang, *Nano Energy* **2015**, 15, 125.
- [60] C.-E. Cheng, Z. Pei, C.-C. Hsu, C.-S. Chang, F. Shih-Sen Chien, *Sol. Energy Mater. Sol. Cells* **2014**, 121, 80.
- [61] F. Tan, S. Qu, Q. Jiang, J. Liu, Z. Wang, F. Li, G. Yue, S. Li, C. Chen, W. Zhang, Z. Wang, *Adv. Energy Mater.* **2014**, 4, 1400512.